Surface effects in zinc oxide nanoparticles

Nicolas Combe, Pierre-Marie Chassaing, François Demangeot

Surface effects in zinc oxide nanoparticles

Nicolas Combe,* Pierre-Marie Chassaing,† and François Demangeot‡
CNRS, CEMES (Centre d'Elaboration de Matériaux et d'Etudes Structurales), BP 94347, 29 rue J. Marvig, F-31055 Toulouse, France
Université de Toulouse, UPS, F-31055 Toulouse, France

(Received 18 June 2008; revised manuscript received 3 December 2008; published 12 January 2009)

Structural properties of zinc oxide nanoparticles are theoretically studied focusing on the effects induced by the surfaces. In this aim, we compare two models: an atomistic and an elastic model. Atomistic model uses a semiempirical potential: the shell model. Effects of surface relaxation and surface stress are taken into account in this model while they were not in the elastic model. Studying nanoparticles with sizes varying from 1.5 to 4.5 nm, we show that surface relaxation occurs on a typical length of about 1 nm in the vicinity of surfaces within the atomistic model. This significant length is due to the existence of long-range interaction forces in zinc oxide which is an ionocovalent material. Because this typical length is comparable to nanoparticle size, elasticity fails to reproduce correctly structural properties of the nanoparticles. As an illustration of structural properties changes by decreasing nanoparticles sizes, we study the nanoparticles acoustic vibrations eigenfrequencies focusing on the mostly observable modes by vibration spectroscopy. Differences between elasticity and atomistic calculations are attributed to surface effects. If elasticity acceptably provides vibration frequencies of most studied nanoparticles, it fails to reproduce them for nanoparticles with a size below an approximate value of 2.5 nm. We expect such effects to be experimentally observable.

DOI: 10.1103/PhysRevB.79.045408 PACS number(s): 78.67.Bf, 63.22.−m, 68.35.Gy

I. INTRODUCTION

Decreasing the size of nanoparticles (NPs) or quantum dots increases their surface/volume ratio. The effect of the surface can then become predominant and allows to access new material properties.[1] Especially, increasing surface/volume ratio in NP raises fundamental questions related to mechanical properties and to the localized and discrete nature of the electronic and vibrational states.[2] For instance, the effect of confinement on the electronic properties in quantum dots has been demonstrated more than a decade ago, in the case of InAs.[3] In this study, we aim to quantify the effects due to surface on the structural properties of NPs. To understand how the presence of surface can modify the structural properties, let us first write a few lines of thermodynamics. The free-energy differential for an infinitesimal modification of a freestanding NP shape at constant entropy and number of atoms reads:

$$\mathbf{d}F = \int\int\int_{\mathcal{V}} \sigma_{ij}\delta\epsilon_{ij}d\mathcal{V} + \int\int_{\mathcal{A}} \tilde{s}_{\alpha\beta}\delta\epsilon_{\alpha\beta}dS + \gamma\mathbf{d}\mathcal{A}, \quad (1)$$

where $\mathcal{A}$ and $\mathcal{V}$ are the surface and volume of the nanoparticle. The symbol **d** corresponds to a differential and is thus related to the infinitesimal shape changes, whereas the symbol d is related to integrations. $\delta\epsilon_{ij}$ denotes the infinitesimal bulk deformation. The first term represents the volumic elastic term. $\bar{\bar{\sigma}}$ and $\bar{\bar{\epsilon}}$, respectively, design the stress and strain tensors. The second term represents the free-energy variation by the surface deformation of the NP.[4–7] $\tilde{s}$, called the surface stress tensor, designs the excess of tangential components of the stress tensor and $\tilde{s}_{\alpha\beta}\mathbf{d}\epsilon_{\alpha\beta}dS$ is the elastic excess energy at the surface.[8] The last term represents the free-energy variation by creation of surface; γ is the well-known surface energy. We decompose here the surface excess energy as the sum of two terms:[5,7] the term $\int\int_{\mathcal{A}}\tilde{s}_{\alpha\beta}\delta\epsilon_{\alpha\beta}dS$ coming from the deformation of the surface (at constant surface atoms) and the term $\gamma\mathbf{d}\mathcal{A}$ coming from the creation (at constant strain) of the surface. The surface stress tensor is related to the surface energy through the Shuttleworth's relation.[9]

Let us now imagine a freestanding nanoparticle which we want to know the equilibrium shape of. This NP is only submitted to its internal forces; the equilibrium shape corresponds to the minimum of free energy compared to infinitesimal NP deformation. Such deformations are expected to be small enough, so that no plastic deformation occurs. In this case, the number of surface atoms remains constant implying no creation of surface. The last term of Eq. (1) is thus cancelled and surface effects only reveal through the deformation surface term.

Surface stress is well known in surface physics for inducing phenomena such as reconstruction, interfacial mixing, segregation, and self-organization. The Laplace law $\Delta P = \frac{2\bar{s}}{R}$ for solid NPs is one of its consequences.[10,11] ΔP is the difference between the inside and outside pressures, $\bar{s}$ characterizes the surface stress, and R is the local surface curvature. The existence of surface stress may induce a volumic strain in the NPs. This deformation is all the more important since the ratio surface/volume in the NP is high.

Surface stress induces an inhomogeneous strain field in a NP. Let us call λ the characteristic depth beneath the surface over which surface effects are significant. This length characterizes the surface relaxation. At the atomic scale, we expect this typical length to be of the order of the atomic interaction range, i.e., about a few angstroms to 1 nm. If this typical length becomes of the same order as the NP size, we expect a strong deformation of the NP and thus a strong alteration of its structural properties.

Therefore, it is judicious to choose a material with a typical length λ as large as possible, so that these effects may experimentally be observable. We thus choose to study zinc oxide (ZnO), an ionocovalent compound that ensures long-range interactions between atoms. ZnO is currently the aim

of many research projects in view of a widespread range of applications.[12,13]

In this paper, we will theoretically study the surface effects on ZnO NPs. NPs are freestanding wurtzite ZnO prisms identical to the ones experimentally synthesized by a one-step wet chemistry method.[14] Prisms are faceted with hexagonal basis of diameter d and height h. Each NP has an aspect ratio h/d depending on experimental conditions. Typical experimental sizes (height or diameter) vary from 2 to 7 nm. The choice of prismatic shape also corresponds to the symmetry of the hexagonal lattice and is a good approximation of the Wulff equilibrium shape for hcp crystals.[15]

To describe the effects of the surface, we compare structural properties of ZnO NPs using two models: the linear elasticity theory without any surface stress and an atomistic model based on a semiempirical potential. Actually, linear elasticity theory can handle surface stress [following Eq. (1)], but surface stress determination asks experiments or atomistic calculations.[16] In addition, surface stress in elasticity theory does not consider the typical range λ of surface relaxation; indeed, the precise physical meaning of an excess quantity such as surface elastic energy is to compact the surface effects (which can spread in the vicinity of the surface) in a quantity characteristic of the surface. For these reasons, the elasticity theory is used in this study without any surface terms. On the contrary, atomistic calculations implicitly take into account surface effects. Differences between structural properties computed with these two models will thus reveal effects due to the surface stress and surface relaxation. Using the atomistic model, we are able to compute structural properties of NPs of size varying from 1.5 to 4.4 nm, i.e., in the range of experimental sizes. The same calculation using linear elasticity theory does not suffer from any size limitations.

Experimentally, mechanical properties of NPs can efficiently be probed by the study of their vibration properties. Among experimental techniques,[17,18] vibration spectroscopy (Raman or time resolved)[19–23] is a nondestructive, fast, and reliable technique to characterize NPs and may thus be able to reveal these surface effects on mechanical properties of NPs. Especially, observable acoustic vibration modes are characterized by a long wavelength that is proportional to the NP size. Changing the size of NPs thus allow to probe the phonon-dispersion diagram and to measure elastic properties. As a matter of fact, in the second part, we illustrate the change in mechanical properties as decreasing the NP sizes by studying the alteration of acoustic vibrations eigenfrequencies by surface effects and the induced inhomogeneous strain field. Surface effects on structural properties of NP have already aroused several studies.

Weissker *et al.*[24] reported the consequences on absorption spectra of the surface reconstruction of Si/Ge nanocrystals. Recently, Ramirez *et al.*,[25,26] studying surface effects on vibration properties of silicon NP, used an atomistic simulation to show a breakdown of frequency-spectra scaling for size smaller than 4 nm. Elasticity forecasts vibration frequencies scale as the inverse of the nanoparticle size. On another side, Combe *et al.*[27] showed that using the Stillinger-Weber potential for germanium, which is another semiconductor, the elasticity describes well the first acoustical vibration frequencies of nanoparticles of size as small as 1 nm.

Concerning metallic compounds, Kara and Rahman[28,29] theoretically studied the vibrational density of states of silver nanocrystal NP showing an enhancement in the vibrational density of states at low frequencies and an overall shift of the high-frequency band beyond the top of the bulk phonons. Meyer *et al.*[11,30] studied the structural properties and the size dependence of capillary pressure and vibration density of state in metallic NPs. The capillary pressure given by the Laplace law holds for particles with a diameter above a critical size of approximately 2.5 nm.

Concerning ionocovalent materials, a recent experimental study of CdSe NPs (Ref. 31) attributes the NP size dependence of structural parameters to surface stress and atomic relaxation related to the presence of stacking faults. Whereas optical vibration properties of ZnO NPs have aroused numerous studies,[32–34] few studies at the atomistic scale deal with structural properties of ZnO NPs and their effects on acoustical vibration properties which is precisely the aim of this paper.

Section II is devoted to the description of the atomistic model including details of computational procedures and to the description of the resolution of the elastic equation. Section III describes the structural properties of NPs using the atomistic description and finally, as an illustration of structural properties changes, Sec. IV presents the comparison between vibration frequencies calculated by the atomistic model and the linear elasticity.

II. MODELS

A. Atomistic simulation: Shell model

The modeling of structural properties of ZnO NPs can be performed either by using *ab initio* first-principles calculations or by using classical semiempirical potentials. The computation of these quantities for NPs of size comparable to experimental ones, namely, few nanometers, would clearly be too expensive using the first technique. On another hand, semiempirical potentials provide a good description of static properties, i.e., precisely the domain concerned by our study. Hence we naturally choose to use a semiempirical potential. Erhart *et al.*[35] described a bond order potential for ZnO. Especially, elastic coefficients are very close to experimental ones. However, this model, as stated by its authors, is not suited for the modeling of NPs where the surface atoms on volume atoms ratio may become on the order of 1.

Other semiempirical potentials belong to the shell-model category. Atoms are ionic and modeled by a core and a shell. Pairwise shells experience a Born-Mayer potential. Coulomb forces couple all entities (core or shell) except the shell and the core belonging to the same ion which interact through a harmonic spring. We found two sets of parameters available for the modeling of ZnO in the literature: one from Binks[36] and one from Lewis and Catlow (LC).[37] We tested both of them. We found that the set of parameters from Binks acceptably reproduces interatomic distances, primitive cell volume, and elastic coefficients but fails to reproduce the phonon-dispersion curves of ZnO and especially the optical part. This discrepancy on optical phonons would in principle not be an issue for the modeling of static properties; however, it re-

TABLE I. Lattice parameters, density, cell volume and elastic coefficients of bulk ZnO calculated using the shell model of Lewis and Catlow compared to experimental data (Refs. 38–40). Elastic coefficients are expressed in gigapascal.

	LC model	Expt.
a (Å)	3.29	3.242
c (Å)	5.09	5.188
Density (g cm^{-3})	5.71	5.6
Cell volume (Å^3)	47.35	47.77
C_{11}	233.66	209.7
C_{12}	110.42	121.1
C_{13}	103.51	105.1
C_{33}	185.90	210.9
C_{44}	72.84	42.5
C_{66}	61.61	44.3

veals an incorrect description of the atomic polarizabilities. Hence, we preferred to use the LC potential which acceptably reproduces optical-phonon-dispersion diagram. Although this potential has been designed in the 1980's, it is still used as a reference potential for ZnO.[35]

1. Bulk properties: Validation of the model

Table I sums up the primitive cell properties and the elastic coefficients obtained by the LC potential for wurtzite ZnO and their corresponding experimental values. These quantities have been computed using the program GULP.[41–43] Computed quantities show a very good agreement with experimental ones. Note that first-principles calculations using density-functional theory (DFT) [local-density approximation (LDA) and generalized gradient approximation (GGA)] reproduce experimental data with about the same precision.[44,45] The phonon-dispersion diagram for the LC model correctly reproduces the experimental dispersion diagram.[35] Especially, due to the good agreement between the computed and experimental stiffness tensor, the low-frequency acoustical branches are well modeled. Note that since we will focus on acoustic vibrations of NPs at the end of the study, this agreement supports the relevance of the LC model.

2. Nanoparticles: Stabilization of polar surfaces

In this work, we aim to simulate nanostructures of ZnO with a prismatic shape as synthesized experimentally.[14] The prism axis is parallel to the c axis of the wurtzite lattice. We design a prismatic NP with a hexagonal crystal structure.

Side surfaces of the prism are $(1\bar{1}00)$ facets. Two kinds of side surfaces can be exhibited: one where surface oxygen or zinc atoms have two first-nearest neighbors on the surface (only one in projection along the c axis) and one where they have three (two in projection along the c axis). Figure 1 illustrates these two surfaces. Only the second type of surface has been investigated while the first type has been found to be unstable against surface reconstruction using the LC model after minimization of the potential. The studied surface type agrees with some recent density-functional theory calculations on ZnO nanowires.[46]

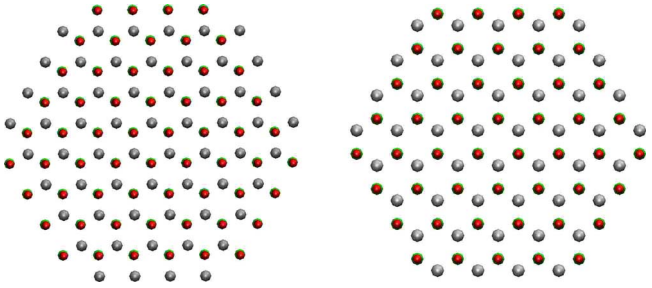

FIG. 1. (Color online) Two kinds of $(1\bar{1}00)$ surfaces before relaxation. On the left figure, surface oxygen or zinc atoms have two first-nearest neighbors (only one in projection along the c axis), whereas they have three on the right one (two in projection along the c axis). Zn and O atoms are, respectively, denoted in gray and red. These two figures represent two NPs of 1320 (left) and 864 (right) atoms projected along the (0001) direction before the minimization of the potential. Configurations of the first type (left figure) have been found to be unstable against surface reconstruction after minimization of the potential.

Top and basis surfaces of the prism are (0001) and $(000\bar{1})$ surfaces. "Tasker type 3"[47] ZnO (0001) and $(000\bar{1})$ surfaces exhibit a nonzero dipole moment perpendicular to the surface. The alternation of oxygen and zinc layers creates a dipole that increases monotonically as a function of the crystal thickness and gives rise to a surface instability. Two main stabilization mechanisms of polar ZnO surfaces have been proposed: (1) reconstruction of the surface and (2) metallization of the surface by charge transfer. Recently, experimental studies[48] using atomic force microscopy corroborate theoretical predictions[49] based on DFT calculations. They show that infinite surfaces are stabilized by mechanism (1) involving a triangular structure. The triangular structure reconstruction in infinite (0001) and $(000\bar{1})$ surfaces is obtained by the removal of one fourth of surface atoms.

In this work, in addition to the necessary stabilization of the polar surfaces, we are constrained by the neutrality of the NP and by the fact that the number of (0001) and $(000\bar{1})$ surface atoms is not necessarily a multiple of 4. Hence, the design of neutral NPs with a triangular structure reconstruction on (0001) and $(000\bar{1})$ surfaces, which incidentally has not been demonstrated nor precisely described in NPs, becomes a very subtle art. For these reasons, we have decided to stabilize the polar surfaces by charge transfer. Zn-terminated surfaces are less positive and O-terminated surfaces are less negative by a factor that converges toward 0.75 with increasing NP size.[50,51] The stabilization mechanism will not crucially affect the structural properties of the NP. Reconstruction and charge transfer both imply a modification of the charge density in the vicinity of (0001) and $(000\bar{1})$ surfaces. This charge peculiarity extends over two monolayers in the first case whereas over one in the second to be compared to the NP size.

TABLE II. Characteristics of the studied nanoparticles. Size is defined as size=$(hd^2)^{1/3}$ in Sec. IV B. Surface atoms are atoms whose number of first neighbors is different from the one in the bulk.

h (nm)	d (nm)	Size (nm)	Aspect ratio	N_{atoms}	Surface atoms
1.54	1.76	1.68	0.875	567	73.0%
2.06	2.45	2.31	0.92	864	59.7%
2.58	2.45	2.49	1.15	1056	56.8%
3.09	3.15	3.13	0.93	1950	48.0%
3.61	3.83	3.76	1.00	3240	41.5%
4.12	4.50	4.37	1.06	4998	36.5%

3. Methodology

Using a conjugate gradient algorithm, the NPs previously constructed are then relaxed by minimizing the overall potential energy to reach their equilibrium states. Our model omits the possible existence of surface reconstructions and dangling bonds. These aspects could correctly be addressed using more sophisticated techniques (for instance DFT or tight binding). Structural properties of NPs can then be calculated.

Concerning the phonon calculations, the dynamical matrix is computed and diagonalized to obtain eigenfrequencies and eigenvectors. The potential minimization procedure ensures that all vibration eigenfrequencies are real. We study in this work NPs with up to 5000 atoms, corresponding to sizes up to 4.4 nm. Table II reports the characteristics of the studied NP.

B. Continuum model: Elasticity

As already mentioned, calculations of structural properties of NPs using elasticity theory are done without any surface stress, so that only the first term in Eq. (1) remains. The NPs are constructed following the same scheme as for the atomistic model. However, NPs constructed from the bulk are in their equilibrium states for elasticity theory. The presence of surfaces in the NPs does not induce any volumic strain or stress since stress and strain in the NPs are uniformly null.

Concerning vibrations, phonon modes are calculated using the elastic coefficients obtained from the LC model in Table I. Eigenvectors displacement field $\vec{u}$ are solutions of the Navier equation in the scope of the linear elasticity theory

$$\rho\omega^2 u_i + \sum_{jkl} C_{ijkl} \frac{\partial^2 u_k}{\partial x_l \, \partial x_j} = 0, \tag{2}$$

where ρ is the volumic mass, ω is the eigenfrequency, u_i is the ith component of the displacement field $\vec{u}$, and $\mathbf{C}$ is the fourth-order stiffness tensor. We compute acoustic vibration eigenfrequencies and eigenmodes using the scheme of Visscher *et al.*[52] The advantage of this scheme is the possibility to solve the Navier equation for any geometry including the elastic coefficients anisotropy. Visscher *et al.* proposed to expand the displacement field of eigenvectors on a polynomial basis. Resolution of Eq. (2) reduces then to matrix algebra. We use in this study polynomials of order up to 11 to ensure the precision and convergence of the method. Eigenfrequencies of the acoustic modes we will study remain unchanged by increasing the base above polynomials of order 11.

Vibrations of a free spherical particle were first studied by Lamb.[53] The case of isotropic elastic spheres embedded in a matrix has also been explored.[54–58] Yadav *et al.*[19] applied the Lamb theory to ZnO spherical NPs for comparison with experimental values; in the isotropic elasticity approximation (which is usually made), for a spherical NP of radius r, the eigenfrequency of a given mode scales as r^{-1}. This power law can easily be understood and extended to the case of anisotropic elastic coefficients. Normalizing spatial coordinates x_i by the typical size χ_i of the NP in that direction $x_i' = \frac{x_i}{\chi_i}$, Eq. (2) reads

$$\rho\omega^2 u_i + \sum_{jkl} \frac{C_{ijkl}}{\chi_l \chi_j} \frac{\partial^2 u_k}{\partial x_l' \, \partial x_j'} = 0. \tag{3}$$

In the case of a spherical NP, all typical sizes χ_i are equal and proportional to the sphere radius r, so that for a given mode, ωr becomes independent of the NP radius even for anisotropic elastic coefficients. This power law has been experimentally checked on spherical NPs using vibration spectroscopy in numerous studies.[59–63]

In our case, prismatic NPs have two typical sizes: their diameter d and their height h. The expression of the frequency ω as a function of d and h for a given mode is certainly very complex and at least far from being obvious. However, if we compare prismatic NPs at constant aspect ratio $\frac{h}{d}$, linear elasticity theory predicts again that ωd becomes independent of the NP size. For this reason, we will only study in Sec. IV vibration properties of NPs with aspect ratio (around) unity as shown in Table II.

III. STRUCTURAL PROPERTIES OF NANOPARTICLES

In this section, we discuss the equilibrium layout of NPs in the scope of the atomistic model compared to linear elasticity. As already mentioned, NPs constructed from the bulk are in equilibrium state in the scope of the elasticity model; thus, the comparison of displacement fields before and after relaxation in the scope of the atomistic model provides a direct comparison between the elastic and atomistic models. In the following, we consider a NP of 3.09 nm height and of 3.15 nm diameter, which is an intermediate size in our calculations and we describe it using cylindrical coordinates, with the z axis being the c axis of the hcp crystal, and the origin ($r=0$, $z=0$) is at the NP center of mass. Atoms, initially located as in bulk ZnO as represented in Fig. 2 (left), relax to the final structure shown on the right part of Fig. 2 by minimization of the interatomic potential. The relaxed NP is constricted in the $z=0$ plane and extended along the z axis. We precisely define the diameter and height of the NP as it would be measured experimentally, i.e., on the relaxed NP.

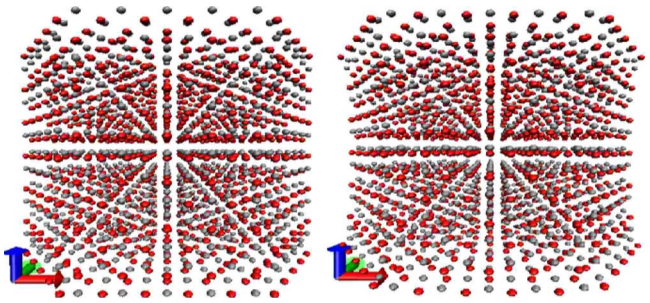

FIG. 2. (Color online) Perspective view along the $[1\bar{1}00]$ direction of a 3.09-nm-height and 3.15-nm-diameter ZnO nanoparticle before (left) and after (right) relaxation. Zn and O atoms are denoted in gray and red, respectively. Blue axis denotes the z axis parallel to the c axis of the hcp crystal structure.

The diameter is the largest distance between atoms in the $z=\pm h/2$ plane. The height is the largest vertical distance between atoms along the z axis.

Figure 3 presents the atomic displacements consecutively to the NP relaxation occurring along radial and axial directions (noted u_r and u_z, respectively) plotted vs r and z coordinates. Evaluation of the strain tensor inside the NP could easily be deduced from the displacement field using $\varepsilon_{rr}=\frac{\partial u_r}{\partial r}$, $\varepsilon_{zz}=\frac{\partial u_z}{\partial z}$, and $\varepsilon_{rz}=\frac{1}{2}(\frac{\partial u_r}{\partial z}+\frac{\partial u_z}{\partial r})$. We choose to represent here the displacement field rather than the strain tensor to avoid a numerical derivation and to facilitate the interpretation.

Figure 3(a) shows that in the $z=0$ plane, atoms are all the more constricted as they are located near the side surface

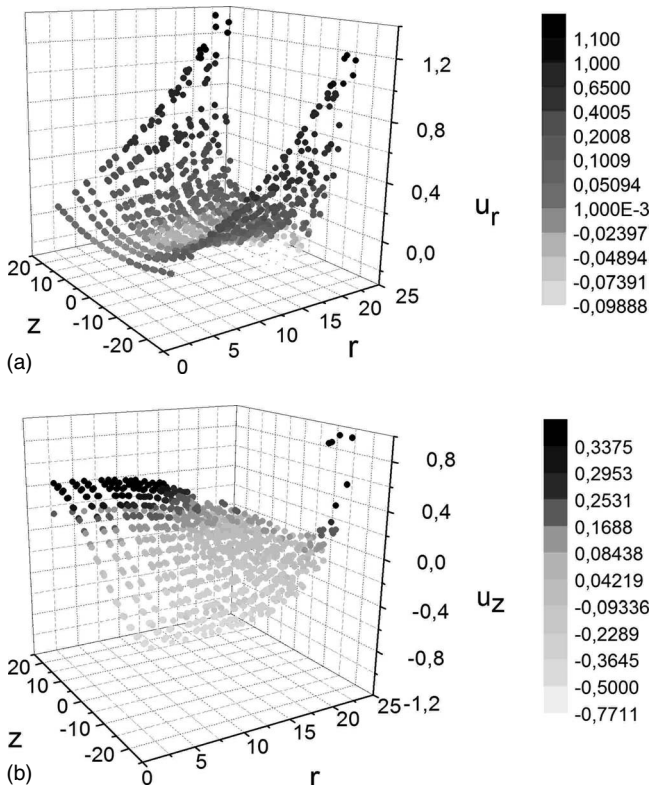

FIG. 3. Atomic displacements along (a) the radial direction and (b) the z direction vs r and z coordinates for a 3.09-nm-height and 3.15-nm-diameter NP. All quantities are in angstrom.

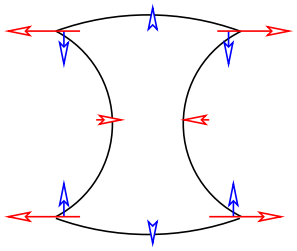

FIG. 4. (Color online) Sketch of the relaxed NP shape.

$r=d/2=15.7$ Å. In addition, this map also reveals that atoms near the (0001) and $(000\bar{1})$ surfaces have extended from the z axis of the NP. This extension increases with the radial position of the atom. Figure 3(b) reports atomic displacements along the z axis. Atoms located near the edges of the (0001) and $(000\bar{1})$ surfaces significantly move toward the $z=0$ plane whereas atoms in the core of the NP are moving in the opposite direction. Note that both Figs. 3(a) and 3(b) suggest atomic displacements up to about 1 Å. The displacement field revealed by Fig. 3 leads to a NP shape that is illustrated in Fig. 4. In Fig. 3, we consider a NP of 3.09 nm height and of 3.15 nm diameter. For smaller NPs, atomic displacements and surface effects become more important due to a greater surface/volume ratio but the qualitative description remains.

Figure 3 clearly shows a non-negligible displacement field even in the core of the NP. The atomic interactions induce a surface relaxation in the vicinity of the surface. To quantify the typical length of this relaxation in ZnO, Fig. 5 (top) plots the radial displacement field as a function of r in the $z=0$ plane for the biggest NP we can afford. This procedure ensures that the (0001) and $(000\bar{1})$ surfaces minimally interfere on atom displacements. Figure 5 reveals that surface relaxation in the plane $z=0$ induces an almost linear displacement in the NP core. The NP core is uniformly strained in volume with a typical value of $\varepsilon_{rr}=0.3\%$ (for the 4 nm NP). Note that such a uniform strain is compatible with

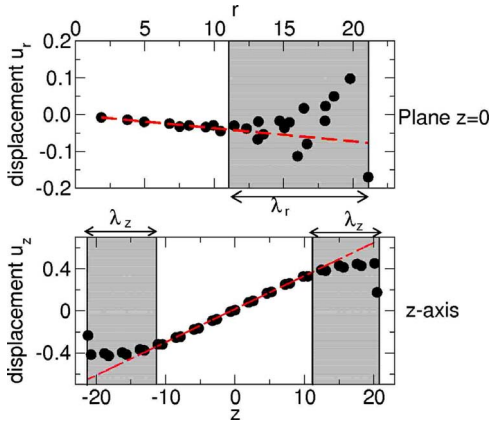

FIG. 5. (Color online) Zn and O displacement fields along radial direction (top) in the plane $z=0$ and along vertical direction (bottom) in the subspace $r=0$ for a 4998 atom NP ($h=4.0$ nm and $d=4.3$ nm). r and z are reported in angstrom. Regions where surface relaxation is significant are patterned. Dashed line is a linear regression of the displacement field in the NP core.

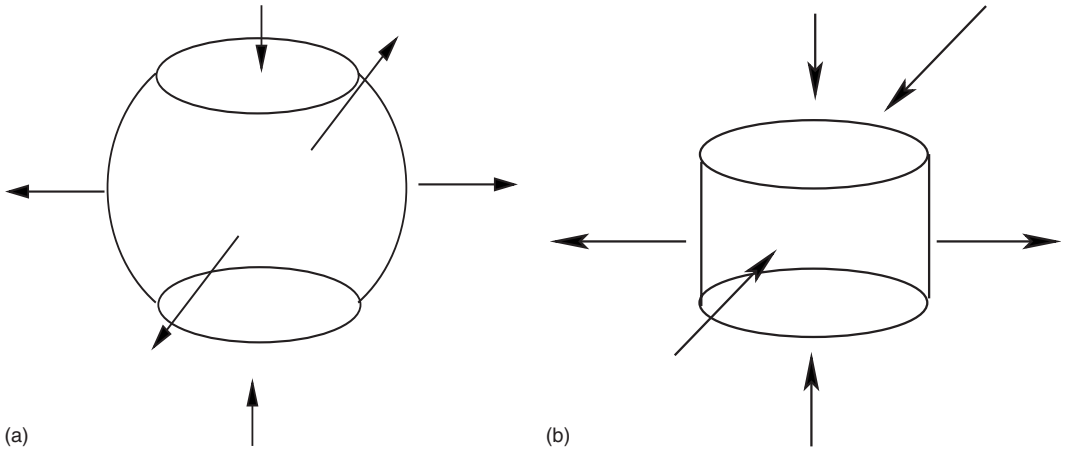

FIG. 6. Schematic illustration of the extensional (left) and peanut (right) modes.

the Laplace law mentioned above.[11] In ZnO, the typical length scale characterizing the surface relaxation is measured after removing the linear part of the displacement field (not shown). We find $\lambda_r \approx 1$ nm. An analogous protocol is used on the z axis in Fig. 5 (bottom) to quantify the relaxation of (0001) and $(000\bar{1})$ surfaces. We find $\lambda_z \approx 1$ nm and a typical value of $\varepsilon_{zz}=3\%$ in the core of the NP.

As a matter of fact, we can expect a significant effect of surface relaxation on experimentally measured structural properties of NP when size and surface relaxation length turn to be of the same order of magnitude, i.e., $r=\lambda_r=1$ nm; indeed, for a NP of 2 nm diameter and of 2 nm height, the surface relaxation involves 100% of the volume of the NP. Note that for NP of radius $r=3\lambda_r=3$ nm the surface relaxation already involves about $\frac{h\pi r^2-(h-2\lambda_z)\pi(r-\lambda_r)^2}{h\pi R^2}=70\%$ of the volume of the NP. In Sec. IV, we illustrate these structural properties changes by the study of acoustic vibration properties of these NPs.

IV. ACOUSTIC PHONONS

A. Observable vibration modes

Vibration spectroscopy[59–63] is able to check the eigenfrequencies power-law scaling as r^{-1} for a spherical NP of radius r. In this part, we illustrate the modification of structural properties of ZnO nanoparticles by analyzing their vibration eigenfrequencies size dependence. Yadav *et al.*[19] studied by Raman scattering the acoustic vibration modes of ZnO spherical NPs with diameter varying from 5 to 10 nm. In a homogeneous elastic sphere, the most studied case, eigenmodes can be separated into two categories: spheroidal and torsional modes. Essentially, spheroidal modes are observable by Raman or time-resolved spectroscopy. In the following, among the thousands eigenmodes of a NP, we focus on two spheroidal modes: the breathing ($l=0$ and $n=1$ using Yadav *et al.*[19] notations) and quadrupolar modes ($l=2$ and $n=1$) since they are the most observable modes by the cited experimental techniques because of their high interaction with electronic states via potential deformation mechanism. Note that time-resolved experiments are sensible to the breathing mode, while Raman spectroscopy detects both breathing and quadrupolar modes.[64]

The quadrupolar mode of a sphere consists in a biaxial constriction of a planar section of the sphere while the orthogonal direction of the plane is expanding, and vice versa. The breathing mode consists in a succession of isotropic extensions/constrictions of the whole sphere.

When studying prismatic NPs, we consider the two following modes derived from the quadrupolar mode of an isotropic sphere: (i) if the extension occurs in the $z=0$ plane then the constriction is axial, this mode is called the extensional mode, and (ii) if the constriction is in a $\theta=C^{st}$ plane, the extension is in $\theta'=C^{st}+\pi/2$ direction. From a top view of this mode the particle would look like a peanut; we call this mode the peanut mode. Figure 6 illustrates schematically both extensional and peanut modes. In addition, we consider a breathing mode of a prismatic NP (aspect ratio unity) which is similar to the one of a sphere. Note that analytical calculations of NP vibration modes have never been performed in a prism but in a close geometry, namely, the cylinder. However, these calculations most often assume an infinitely long cylinder and isotropic elastic coefficients[65,66] which can obviously not be compared to our prism of aspect ratio unity with an hcp crystal structure.

Visscher *et al.*[52] method allows a precise calculation of the vibration eigenfrequencies of a prism. We find that the three modes' breath, extensional and peanut frequencies are not degenerated. Especially, the anisotropic shape breaks the degeneracy of the peanut and extensional mode frequencies (that exists in an sphere with elastic isotropy). Moreover, this breaking is reinforced by the anisotropy of the stiffness tensor of ZnO.

Atomistic calculations confirm this point. In the case of $h=3.09$ nm and $d=3.15$ nm NP, the extensional mode was found at $\omega_{ext}=26.0$ cm^{-1}, while the peanut mode was found at $\omega_{pea}=26.7$ cm^{-1}. However, experimentally, since acoustic phonons peaks of NPs have a typical full width at half maximum of ~ 10 cm^{-1} in Raman spectra[19] (mainly due to inhomogeneous broadening), the splitting between extensional and peanut modes could hardly be observable by Raman spectroscopy for such NP. Only for very small NPs (typically ≤ 2.0 nm), we find $\omega_{ext}=35.6$ cm^{-1} and $\omega_{pea}=40.0$ cm^{-1} ($h=2.06$ nm and $d=2.25$ nm). The difference becomes significant.

TABLE III. Comparison between breathing and quadrupolar mode frequencies of spherical NP (d=3.4 nm) derived from Eqs. (7) and (8) of Ref. 19 and breathing, extensional, and peanut modes of prismatic NP (h=3.09 nm and d=3.15 nm).

Sphere		
	ω_{br}^{sph} (cm^{-1})	ω_{quad}^{sph} (cm^{-1})
Eqs. (7) and (8) of Ref. 16	55.9	22.1

Prism			
	ω_{br} (cm^{-1})	ω_{ext} (cm^{-1})	ω_{pea} (cm^{-1})
Atomistic	55.9	26.0	26.7
Elasticity (Visscher)	56.5	23.3	24.8

In the following, we will focus on the breathing and extensional mode since observation of both peanut and extensional modes may experimentally be arduous. Orders of magnitude of eigenfrequencies of prism vibrations calculated using both atomistic calculations and elasticity theory can be compared to values obtained from Eqs. (7) and (8) of Ref. 19 giving the breathing and quadrupolar mode frequencies of ZnO spherical NP. These last equations satisfactorily describe experimental values for NPs whose diameters exceed 5 nm. Following these equations, the breathing and quadrupolar mode frequencies of a 3.4-nm-diameter spherical NP would be ω_{br}^{sph}=55.9 cm^{-1} and ω_{quad}^{sph}=22.1 cm^{-1}. Using the atomistic description with a prismatic NP involving the same volume h=3.09 nm and d=3.15 nm, the breathing and the extensional mode frequencies are, respectively, 55.9 and 26.0 cm^{-1}. Linear elasticity (through Visscher scheme) provides 56.5 and 23.3 cm^{-1}. Table III sums up this comparison.

Observation of Table III reveals that both calculations in the framework of the shell model and the theory of elasticity lead to frequencies which are close to those measured by Raman-scattering experiments. This point is an important result that supports the relevance of our calculations. In addition, both shell model and theory of elasticity provide frequencies in a close proximity for a 3.4 nm NP. We now analyze how these frequencies vary with the NP size.

B. Atomistic vs elastic model

In the following, we compare the size dependence of breathing and quadrupolar mode frequencies computed by the atomistic and elastic models. Identification of modes has been performed using a systematic projection of atomistic modes on elastic ones and using a careful analysis of the displacement fields of modes. As explained in Sec. II B, vibration mode frequencies follow a 1/size power law in the elastic model as soon as only one characteristic length exists in the NP, which requires a fixed aspect ratio. The characteristic size of the NP is defined as size=$(hd^2)^{1/3}$.

If fixing the aspect ratio to unity is not an issue in the elastic model, it may not be the case using the atomistic description. Heights and diameters are discrete and are chosen so as not to lead to a surface reconstruction after relaxation (see Sec. II A 2). Therefore, and especially for very small NP, aspect ratio may not exactly match unity (1.15 in the worst case in Table II).

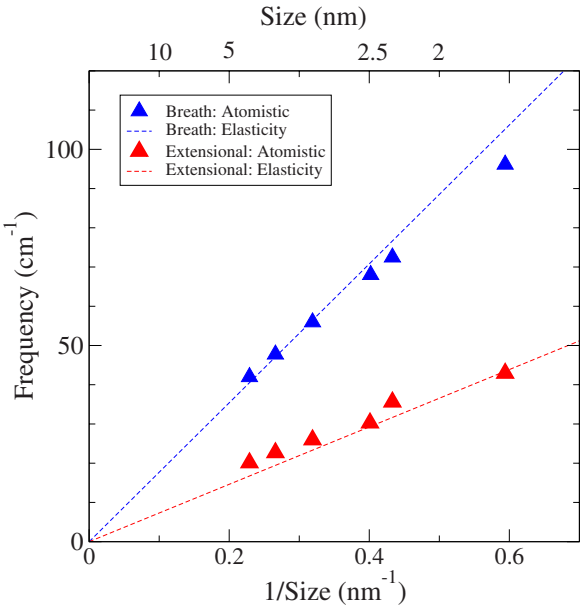

FIG. 7. (Color online) Frequencies of the breathing and extensional modes vs 1/size deduced from both atomistic and continuous models.

Figure 7 reports the breathing and extensional mode frequencies calculated both in the atomistic approach and the elasticity theory. Atomistic calculations were performed on NPs up to size=4.37 nm (h=4.12 nm and d=4.50 nm), which corresponds to ~5000 atoms. The global agreement between atomistic and elasticity models is rather good.

Focusing on the breathing mode, Fig. 7 reveals that ω_{br} is satisfactorily described by the theory of elasticity above an approximate characteristic size of 2.5 nm. The difference between the elastic and atomistic calculations is not significant for larger NPs. ω_{br} in the case of atomistic calculations is ~1.6 cm^{-1} higher than in the case of the elastic model for the 4.4 nm NP. However, this difference becomes significant when reducing the NP size. For smaller NPs, ω_{br} evaluated by atomistic model is found 9 cm^{-1} lower than by linear elasticity. Thus, calculating ω_{br} by means of the theory of elasticity, one would commit a ~10% error on the value of ω_{br} for a 1.5-nm-size NP. Note that experimental setup resolution is below 9 cm^{-1}.

On another side, concerning the extensional mode frequencies, atomistic calculations predict a value 3 cm^{-1} higher than the elasticity theory for the largest NP. Surprisingly, the agreement between atomistic model and the elasticity model is better for the smallest NPs.

We emphasize that we take care in our study to use for elastic model the stiffness tensor provided by the LC model. Moreover, we are considering acoustic phonons of typical wavelengths $q \approx 1/\text{size}$, which corresponds in our case to phonons with $q < \frac{1}{5} q_{BZ}$ where q_{BZ} corresponds to the Brillouin-zone border wave vector. In this region of the Bril-

louin zone, the dispersion is linear and well described by a stiffness tensor.

Consequently, we attribute the discrepancy between atomistic and elastic models to the surface effects. We identify three possible mechanisms induced by surface effects that can explain this result.

First, the Laplace law, as long as one can still define a NP core where the strain field is homogeneous, predicts an increase in the pressure (or more rigorously, in the stress tensor) in this NP core. This pressure may induce an increase in vibration eigenfrequencies compared to the unconstrained elastic model. This effect may be disconnected to the other effects described below, investigating NPs whose sizes are much larger than the surface relaxation length λ and whose strain field in the NP is weak compared to the linear elasticity domain limits. Unfortunately, due to computer limitations, we are not able to provide vibration frequencies for bigger particles than 4.4 nm using atomistic simulations.

Second, as already suggested, we expect a modification of vibration eigenfrequencies scaling law due to inhomogeneous strained field in the vicinity of the surface when the surface relaxation length λ becomes comparable to the NP size.

Third, as shown above in Sec. III, when decreasing the NPs size, the strain fields in the NP become comparable (we measured a strain of 3%) to usual linear elasticity limits, so that anharmonic effects may become an issue. In our atomistic study, we use a harmonic description by calculating the dynamical matrix, but we address the anharmonicity of the semiempirical LC potential that can be involved by a significant strain in the NP.

All of these effects are induced by surface effects. Coming back to Fig. 7, if one could hardly think about experimentally detecting surface effects by studying the extensional mode since differences between elastic and atomistic frequencies are not experimentally significant, the study of the breathing mode as a function of 1/size may reveal these surface effects by studying NP of typical size of 2.5 nm and below. Especially, note that the breathing mode frequency is not a linear function of 1/size. Finally, note that a typical size of 2.5 nm is on the order of twice the surface relaxation length, suggesting that the second mechanism mentioned above is dominating.

V. CONCLUSION

We first show that surface effects may involve a significant displacement field in NPs. We describe this displacement field showing how the NP is strained by performing atomistic calculations, a powerful tool that takes into account all surface effects. Although the LC potential certainly fails to reproduce all the characteristics of ZnO systems, we believe that such potential clearly allows a more accurate description of ZnO NPs than elasticity theory. In this study, we have used the theory of elasticity without taking into account surface effects. Artificially including a surface stress in elasticity theory would not presumably[67] help to reduce the discrepancies. A surface relaxation length of about 1 nm can no longer be omitted in ZnO NPs of a few nanometers. It is remarkable that surface effects and especially surface relaxation effects are so significant on strain fields in ZnO NPs. We believe that the long atomic interaction range in ZnO is essential to warrant a high surface relaxation length.

Second, we illustrate surface effects by showing that acoustic vibration eigenfrequencies of NPs can be altered by surface effects. We show that if globally elasticity provides a good description of both breathing and extensional mode frequencies, i.e., elasticity provides these frequencies with an accuracy smaller than the experimental one for most of the studied NPs, elasticity fails to reproduce with the same accuracy the breathing mode frequencies of very small NPs. An important point is that, in the case of ZnO, this failure occurs for typical NP size, on the order of 2.5 nm (breathing mode) available experimentally.[14] Since NPs low-frequency vibration spectroscopy of such small NP is achievable, results presented in this work give reasonable hopes to observe these surface effects experimentally by vibration spectroscopy and especially a nonlinearity in the modes frequencies as a function of the inverse NP size.

In addition, this study may easily be extended to other materials. One can expect the strongest effects of the inhomogeneous strain field in ionocovalent materials (ZnO, ZnS, CdSe, etc.) and small effects in covalent compounds (Si, Ge, etc.), with the case of metals being an intermediate case. This distinction between materials is however only schematic. Sun *et al.*[68] showed a surface relaxation length in gold NPs comparable to the one found in this work whereas Meyer *et al.*[11] found a surface relaxation length of about 0.7 nm in silver nanoparticles. Note however that the inhomogeneity of the strain field in the vicinity of surface is characterized by the surface relaxation length and an amplitude. A detailed comparative study of inhomogeneous strain fields in different materials will thus be welcomed to address this point.

ACKNOWLEDGMENTS

The authors wish to acknowledge L. Saviot, J. Morillo, and V. Paillard for useful discussions and comments.

*combe@cemes.fr
†chassain@cemes.fr
‡demangeo@cemes.fr

[1] A. Hoshino, K. Fujioka, T. Oku, M. Suga, Y. F. Sasaki, T. Ohta, M. Yasuhara, K. Suzuki, and K. Yamamoto, Nano Lett. **4**, 2163 (2004).
[2] W. Cheng, S. F. Ren, and P. Y. Yu, Phys. Rev. B **68**, 193309 (2003).
[3] J. Y. Marzin, J. M. Gérard, A. Izraël, D. Barrier, and G. Bastard, Phys. Rev. Lett. **73**, 716 (1994).

[4] P. Nozières, *Solids Far from Equilibrium* (Cambridge University Press, Cambridge, 1992), p. 1.
[5] H. Ibach, Surf. Sci. Rep. **29**, 195 (1997).
[6] W. Haiss, Rep. Prog. Phys. **64**, 591 (2001).
[7] P. Müller and A. Saúl, Surf. Sci. Rep. **54**, 157 (2004).
[8] Another term involving the strain tensor excess and the stress tensor at the surface usually appears in the expression of *dF*. However, in the following we will only consider NP with free boundary conditions, so that the stress tensor is null at the surface.
[9] R. Shuttleworth, Proc. Phys. Soc., London, Sect. A **63**, 444 (1950).
[10] C. Solliard and M. Flueli, Surf. Sci. **156**, 487 (1985).
[11] R. Meyer, S. Prakash, and P. Entel, Phase Transitions **75**, 51 (2002).
[12] C. Jagadish and S. J. Pearton, *Zinc Oxide Bulk, Thin Films and Nanostructures* (Elsevier, New York, 2006), Vol. 1.
[13] Ü. Özgür, Y. I. Alivov, C. Liu, A. Teke, M. A. Reshchikov, S. Dogan, V. Avrutin, S.-J. Cho, and H. Morkoç, J. Appl. Phys. **98**, 041301 (2005).
[14] M. L. Kahn, T. Cardinal, B. Bousquet, M. Monge, V. Jubera, and B. Chaudret, ChemPhysChem **7**, 2392 (2006).
[15] M. Touzani and M. Wortis, Phys. Rev. B **36**, 3598 (1987).
[16] J. J. Métois, A. Saúl, and P. Müller, Nature Mater. **4**, 238 (2005).
[17] H. Frase, B. Fultz, and J. L. Robertson, Phys. Rev. B **57**, 898 (1998).
[18] U. Stuhr, H. Wipf, K. H. Andersen, and H. Hahn, Phys. Rev. Lett. **81**, 1449 (1998).
[19] H. K. Yadav, V. Gupta, K. Sreenivas, S. P. Singh, B. Sundarakannan, and R. S. Katiyar, Phys. Rev. Lett. **97**, 085502 (2006).
[20] G. Mariotto, M. Montagna, E. D. G. Viliani, S. Lefrant, E. Rzepka, and C. Mai, Europhys. Lett. **6**, 239 (1988).
[21] M. Ivanda, K. Babocsi, C. Dem, M. Schmitt, M. Montagna, and W. Kiefer, Phys. Rev. B **67**, 235329 (2003).
[22] V. A. Fonoberov and A. A. Balandin, Phys. Rev. B **70**, 233205 (2004).
[23] M. A. van Dijk, M. Lippitz, and M. Orrit, Phys. Rev. Lett. **95**, 267406 (2005).
[24] H.-C. Weissker, J. Furthmüller, and F. Bechstedt, Phys. Rev. B **67**, 245304 (2003).
[25] F. Ramirez, P. R. Heyliger, A. K. Rappé, and R. G. Leisure, Phys. Rev. B **76**, 085415 (2007).
[26] F. Ramirez, P. R. Heyliger, A. K. Rappé, and R. G. Leisure, J. Acoust. Soc. Am. **123**, 709 (2008).
[27] N. Combe, J. R. Huntzinger, and A. Mlayah, Phys. Rev. B **76**, 205425 (2007).
[28] A. Kara and T. S. Rahman, Phys. Rev. Lett. **81**, 1453 (1998).
[29] A. Kara and T. S. Rahman, Surf. Sci. Rep. **56**, 159 (2005).
[30] R. Meyer, L. J. Lewis, S. Prakash, and P. Entel, Phys. Rev. B **68**, 104303 (2003).
[31] P.-J. Wu, Y. P. Stetsko, K.-D. Tsuei, R. Dronyak, and K. S. Liang, Appl. Phys. Lett. **90**, 161911 (2007).
[32] K. A. Alim, V. A. Fonoberov, and A. A. Balandin, Appl. Phys. Lett. **86**, 053103 (2005).
[33] V. A. Fonoberov and A. A. Balandin, Phys. Status Solidi C **1**, 2650 (2004).
[34] P.-M. Chassaing, F. Demangeot, V. Paillard, A. Zwick, N. Combe, C. Pagès, M. L. Kahn, A. Maisonnat, and B. Chaudret, Phys. Rev. B **77**, 153306 (2008).
[35] P. Erhart, N. Juslin, O. Goy, K. Nordlund, R. Müller, and K. Albe, J. Phys.: Condens. Matter **18**, 6585 (2006).
[36] D. J. Binks, Ph.D. thesis, University of Surrey, 1994.
[37] G. Lewis and C. Catlow, J. Phys. C **18**, 1149 (1985).
[38] T. B. Bateman, J. Appl. Phys. **33**, 3309 (1962).
[39] J. Albertsson, S. Abrahams, and A. Kvick, Acta Crystallogr. Sect. B: Struct. Sci. **45**, 34 (1989).
[40] E. H. Kisi and M. Elcombe, Acta Crystallogr. Sect. C: Cryst. Struct. Commun. **45**, 1867 (1989).
[41] J. Gale, J. Chem. Soc., Faraday Trans. **93**, 629 (1997).
[42] J. D. Gale, Philos. Mag. B **73**, 3 (1996).
[43] J. Gale and A. Rohl, Mol. Simul. **29**, 291 (2003).
[44] R. Ahuja, L. Fast, O. Eriksson, J. M. Wills, and B. Johansson, J. Appl. Phys. **83**, 8065 (1998).
[45] J. Serrano, A. H. Romero, F. J. Manjón, R. Lauck, M. Cardona, and A. Rubio, Phys. Rev. B **69**, 094306 (2004).
[46] H. Xu, A. L. Rosa, Th. Fraunheim, R. Q. Zhang, and S. T. Lee, Appl. Phys. Lett. **91**, 031914 (2007).
[47] P. W. Tasker, J. Phys. C **12**, 4977 (1979).
[48] F. Ostendorf, S. Torbrügge, and M. Reichling, Phys. Rev. B **77**, 041405(R) (2008).
[49] O. Dulub, U. Diebold, and G. Kresse, Phys. Rev. Lett. **90**, 016102 (2003).
[50] C. Noguera, J. Phys.: Condens. Matter **12**, R367 (2000).
[51] J. M. Carlsson, Comput. Mater. Sci. **22**, 24 (2001).
[52] W. M. Visscher, A. Migliori, T. M. Bell, and R. A. Reinerr, J. Acoust. Soc. Am. **90**, 2154 (1991).
[53] H. Lamb, Proc. London Math. Soc. **13**, 187 (1882).
[54] A. Tamura, K. Higeta, and T. Ichinokawa, J. Phys. C **15**, 4975 (1982).
[55] P. Verma, W. Cordts, G. Irmer, and J. Monecke, Phys. Rev. B **60**, 5778 (1999).
[56] D. B. Murray and L. Saviot, Phys. Rev. B **69**, 094305 (2004).
[57] L. Saviot, D. B. Murray, and M. C. Marco de Lucas, Phys. Rev. B **69**, 113402 (2004).
[58] H. Portales, L. Saviot, E. Duval, M. Fujii, S. Hayashi, N. D. Fatti, and F. Vallée, J. Chem. Phys. **115**, 3444 (2001).
[59] A. Arbouet, N. D. Fatti, and F. Vallée, J. Chem. Phys. **124**, 144701 (2006).
[60] N. Del Fatti, C. Voisin, F. Chevy, F. Vallée, and C. Flytzanis, J. Chem. Phys. **110**, 11484 (1999).
[61] B. Palpant, H. Portales, L. Saviot, J. Lermé, B. Prével, M. Pellarin, E. Duval, A. Perez, and M. Broyer, Phys. Rev. B **60**, 17107 (1999).
[62] A. Diéguez, A. Romano-Rodríguez, A. Vilà, and J. R. Morante, J. Appl. Phys. **90**, 1550 (2001).
[63] A. Tanaka, S. Onari, and T. Arai, Phys. Rev. B **47**, 1237 (1993).
[64] E. Duval, Phys. Rev. B **46**, 5795 (1992).
[65] A. E. Love, *Treatise on the Mathematical Theory of Elasticity*, 4th ed. (Dover, New York, 1944).
[66] M. Mofakhami, H. Toudeshky, and S. Hashemib, J. Sound Vib. **297**, 293 (2006).
[67] Including a surface stress in elasticity theory would particularly complicate the resolution of the Navier equation. However, these difficulties may be overcome using a finite element method.
[68] D. Y. Sun, X. G. Gong, and X. Q. Wang, Phys. Rev. B **63**, 193412 (2001).